Structural, corrosion and mechanical properties of sputtered deposited chromium tungsten nitride ($Cr_{1-x}W_xN$) nanocomposite thin films

Ravi Prakash[1], R. Jayaganthan[2] and Davinder Kaur[1]*

[1]*Functional Nanomaterials Research Lab, Department of Physics and Centre for Nanotechnology, Indian Institute of Technology Roorkee, Roorkee 247667, Uttarakhand, India*
[2]*Department of Metallurgy & Materials Engineering, Indian Institute of Technology Roorkee, Roorkee 247667, India*

*Corresponding author. Tel: (+91) 1332-285407; Fax: (+91) 1332-273560; E-mail: dkaurfph@iitr.ac.in

ABSTRACT

Chromium tungsten nitride ($Cr_{1-x}W_xN$) thin films were successfully deposited on the silicon (100) substrate using dc magnetron reactive co-sputtering. The structural, surface morphological, electrochemical and mechanical properties were studied using X-ray diffraction, field emission-scanning electron microscopy, atomic force microscopy, electrochemical potentiostat and nanoindentation respectively. X-ray diffraction pattern with different atomic concentrations of tungsten ($0<x<0.61$) shows the presence of (111) and (200) orientation. The content of tungsten (W) in these thin films was controlled by varying the power on the W target. A small amount of tungsten addition led to the significant change in the structural, electrochemical and mechanical properties of the $Cr_{1-x}W_xN$ films. The crystallite size varies from 31.1 nm to 15.2 nm with the W content due to variation in nucleation rate and reduction of the self-shadowing effect of the deposition process. Electrochemical properties of these thin films were studied by Tafel polarization curves, which explored the enhancement in corrosion rate due to the higher ratio of real surface area and projected area after a certain amount of W addition. Hardness follows the Hall-Petch relation and tends to increase with the decrease in grain size. Highest hardness 43.18 Gpa and elastic modulus 341.02 Gpa were achieved at the grain size of 15.2 nm in $Cr_{0.48}W_{0.43}N$ thin film. Copyright © 2016 VBRI Press.

Keywords: Magnetron; crystallite size; corrosion rate; nanoindentation; hardness.

Introduction

Binary transition metal nitride thin films of chromium and titanium have been widely used as corrosion and wear resistance protective coatings due to their good mechanical and tribological properties [1]. But in spite of these properties, binary systems are not sufficient for excellent performance in such applications which required more hardness and better oxidation resistance [2]. There is also a degradation of the properties at higher temperature [2-3]. In order to overcome these problems and to enhance the properties like hardness, elastic modulus, surface morphology, corrosion stability, lubrication, adhesion and adjust the parameters such as lattice constant, grain size, orientation, and internal stress, therefore other metals like Ti, Mo, Al, Ta, Si and W are alloyed [4-5]. Due to covering a wide spectrum of physical and chemical properties therefore ternary transition metal nitride thin films are used in variety of applications like decorative, protective and hot corrosion resistive coatings [6].

Chromium nitride (CrN) thin films have high hardness, high toughness, and very good corrosion and wear resistance. Due to its excellent properties, CrN thin films are extensively used as protective coatings for cutting tools [7-8]. So CrN based ternary compound thin films are most promising material regarding future applications [9]. But CrN thin films start to oxidize near about the temperature 700 °C. These thin films can be deposited using various physical vapor deposition techniques such as cathodic arc evaporation [10], ion beam assisted deposition and magnetron sputtering [11]. Magnetron sputtering has more advantage due to high density, homogeneity and good adhesion of deposited films on the substrate that are required for such applications. Protective thin films enhance the lifetime of the tools or machine's parts and prevent the surface from the affecting environments. Extending the applications lifetime and performance can be beneficial to the cost reduction. CrN based ternary coatings like Cr-Mo-N, Cr-Ti-N, Cr-Al-N, Cr-Si-N, and Cr-Ta-N have been successfully deposited [12-14] by several authors.

To date, related studies on the effect of W content in $Cr_{1-x}W_xN$ thin films on the corrosion rate along with mechanical properties are very rare. The main concern of this paper is to study the effect of W addition on the mechanical as well as corrosion properties of CrN. The addition of W atoms in CrN matrix leads to improved microstructure, hardness and operational temperature. The decrement in corrosion rate along with enhanced mechanical properties of CrN thin films on W additional has shown the potential of $Cr_{1-x}W_xN$ in high temperature optical, microelectronic, glass molding, solid lubrication and protective thin film applications.

Experimental

In this study, chromium tungsten nitride ($Cr_{1-x}W_xN$) thin films were deposited on the silicon (100) substrate at 400 °C temperature using reactive dc magnetron co-sputtering (Excel instruments, India), in which two separate targets (Cr and W) were taken. Both the targets were made of very high purity (99.99 %, Excel Metal & Engg Industries, India) with the dimensions of 50 mm diameter and 3 mm of thickness. The substrates were initially cleaned thoroughly in an ultrasonic bath with a mixture of distilled water and trichloroethylene in 4:1 ratio and then washed with boiled acetone. Before deposition, the chamber was evacuated to a base pressure of the order of 10^{-6} Torr and then backfilled with argon and nitrogen gas to desired deposition pressure of 10 m Torr. The target to substrate distance was fixed at 5 cm. No post-annealing was performed after deposition [15]. Both the targets were sputtered in the presence of 50 % Ar and 50 % N_2 gas mixture. The suitable powers were applied to each target to control the composition of the thin films. The target power for chromium was typically set to 80 watt, while tungsten target power was varied. Before every sputtering run, the targets have been pre-sputtered for 5 min in order to ascertain the same state of the targets in every run. Substrate holder was rotated at 20 rpm in a horizontal plane to achieve a uniform film composition and thickness.

The orientation and crystallinity of the film were studied using a Bruker AXS-D8 advanced X-ray diffractometer of CuK_α (1.54 Å) radiations in θ-2θ geometry at a scan speed of 1°/min. To obtain a profile fitting with good signal, polycrystalline silicon powder was used for instrumental correction [16]. The surface morphology and microstructure were studied using field emission scanning electron microscopy (FE-SEM) FEI Quanta 200F and atomic force microscopy (AFM) NT-MDT: NTEGRA model. The compositions of the thin films were determined using the energy dispersive X-ray analysis (EDAX) attachment in the FE-SEM. In order to analyze the corrosion rate of the synthesized $Cr_{1-x}W_xN$ thin film as a function of the W content, an electrochemical experiment was performed for each thin film. The electrochemical measurements were conducted in a 3.5 wt. % NaCl aqueous solution in double distilled water at room temperature by a Gamry instrument; model PCI 4, interface 1000 potentiostat. A corrosion cell with 0.79 cm^2 exposed area is used in which the electrolyte exposed to thin film. There are three electrodes in which thin film acted as a working electrode, while a standard calomel electrode and a platinum rod served as reference and counter electrodes, respectively. The thin films were immersed in the solution for 2 hours until a stable open circuit potential (OCP) was reached. Potentiodynamic polarization test was then carried out with a scan rate of 1 mV/s. Diagrams for Tafel polarization curves were obtained at the voltage ranging from -0.25 to +0.25 V with respect to the OCP. The mechanical properties were measured using the Micro materials Nanotest system (Wrexham, UK) at room temperature. Deposition time for all films was kept at 30 minutes so the thickness of all the samples was almost same. Therefore, the same amount of load (0.5 mN) was applied to all the samples at a constant loading rate of 0.05 mNs^{-1} in order to compare their mechanical properties.

At least 6 independent indentations were performed and the data were averaged to minimize the irrespective noise and variations.
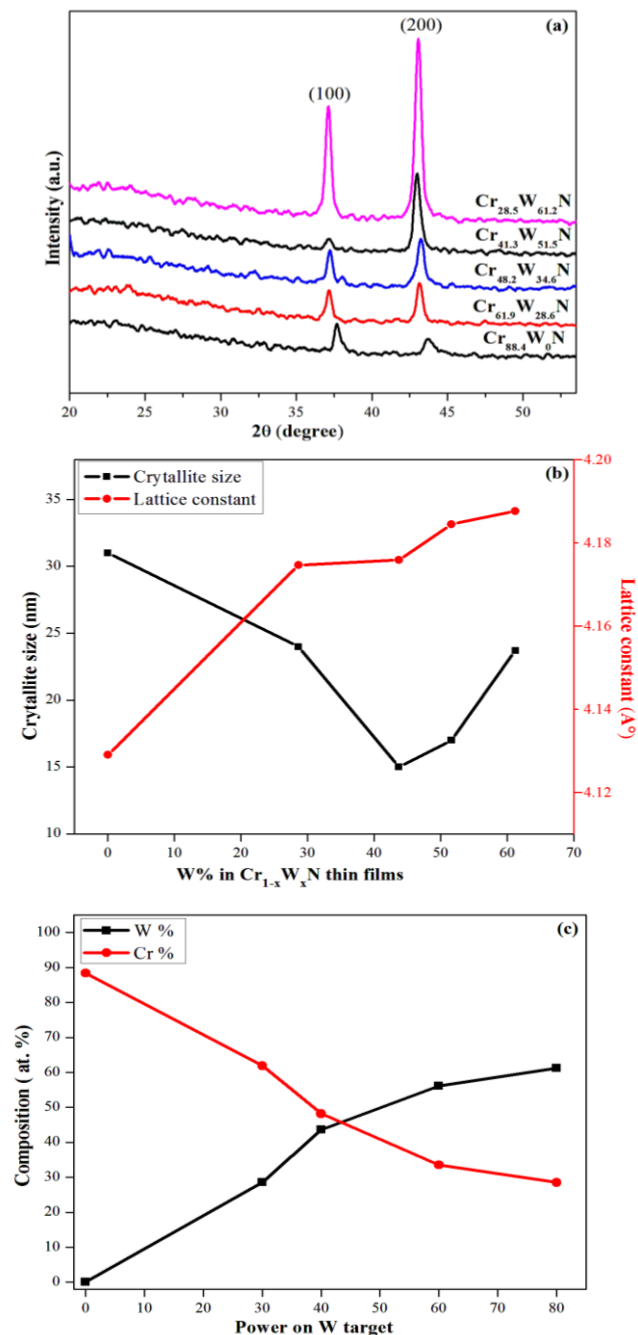
Fig. 1. (a) XRD of all $Cr_{1-x}W_xN$ thin films, (b) Crystalline size and Lattice constant as a function of W % and (c) Relative composition of the Cr, W and N with the power on W target.

Results and discussion

Structural properties, surface morphology and composition

Fig. 1(a) shows the XRD pattern of the $Cr_{1-x}W_xN$ thin films with varying W content onto Si (100) substrate and revealed (111) and preferred (200) reflection which assigned to the fcc B-1 NaCl phase [4, 17]. In XRD pattern, it is also seen that the diffraction peaks of $Cr_{1-x}W_xN$ were shifted towards lower angle side with an increase in W content. This shift indicates the increase in lattice constant

from 4.129 Å to 4.182 Å with the incorporation of W content as shown in **Fig. 1(b)**. Bao-Shun Yau *et al.* [**18**] reported that the enhancement in lattice constant can be explained by the fact that Cr, W and/or N atoms incorporated in interstitial positions and then form a solid solution phase of $Cr_{1-x}W_xN$ so as a result the lattice constant increases.

Scherrer formula Eq. (1) is used to calculate the crystallite size of the $Cr_{1-x}W_xN$ thin films.

$$t = \frac{0.9\lambda B}{\cos\theta} \tag{1}$$

where, t is the crystallite size, λ (1.54 Å) is the wavelength of x-ray, B is FWHM (full width at half the maximum of peak intensity) and θ is the Bragg angle at which the diffraction peak (200) occur. **Fig. 1(b)** demonstrates the variation of crystallite size of $Cr_{1-x}W_xN$ thin films as a function of W content in which crystallite size decreases from 31.2 nm to 15.2 nm with the W addition up to 43.6 % concentration, beyond this W concentration value the crystallite size led to increasing. The reduction of crystallite size may be due to higher kinetic energy and the mobility of the depositing atoms. The kinetic energy of the depositing atoms/molecules depends upon the target power and has been considered as a major factor that decides the adatom mobility and formation of nucleated clusters. High power results, higher sputter rate and higher kinetic energy of depositing atoms, therefore nucleation rate are enhanced and the films with reduced grain size were formed. Thus, grain refinement has been achieved due to increase in nucleation rate with higher magnetron discharge power on tungsten target. As the power on W target reached beyond to 40 watts, the kinetic energy of the incorporated tungsten atoms increases the probability of collision with chromium and nitrogen on the surface of the growing film. Due to collision there could be a sufficient loss of kinetic energy of atoms during deposition, therefore the mobility and diffusion of the atoms become lower and a coarse grain structure would develop, Bao-Shun Yau *et al.* [**18**] and wuhrer *et al.* [**19**] have been reported similar type of results in their study on $Cr_{1-x}W_xN$ thin films.

Table 1. Process parameters for $Cr_{1-x}W_xN$ nanocomposite thin films using reactive dc magnetron co-sputtering.

Deposition process	Reactive dc magnetron co-sputtering
Sputtering target	Cr (99.99%), W (99.99%)
Sputtering power (dc)	Cr (80 watt), W (varied)
Sputtering gas	Pure argon Ar
Reactive gas	N_2
Gas ratio	10:10 sccm
Deposition Pressure	10 m Torr
Deposition time	30 min
Substrate temperature	400°C

Apart from XRD results, the FE-SEM and AFM images also confirmed that grain size of the films decreases to $Cr_{0.48}W_{0.43}N$ thin film and then approaches to increase with the further addition of W content as shown in **Fig. 2**.
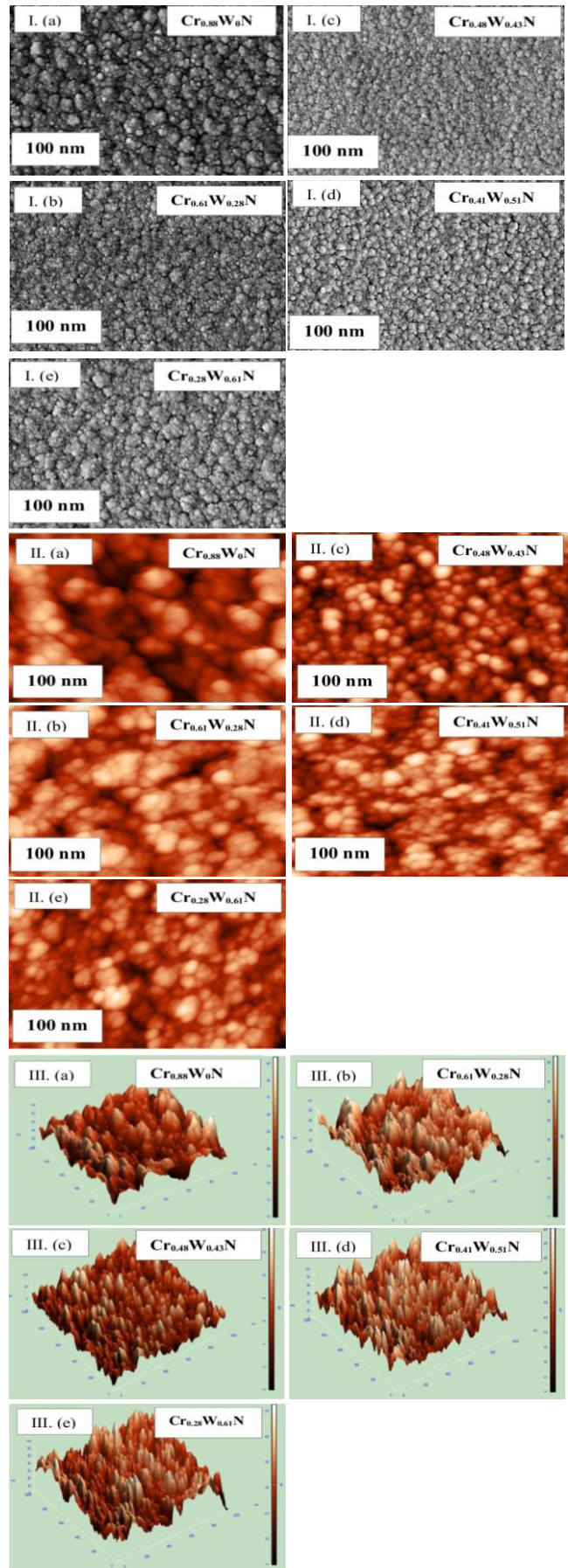
Fig. 2. I (a-e) FE-SEM images, II (a-e) AFM 2-D images and III (a-e) AFM 3-D images of the thin films abbreviated as S-1, S-2, S-3, S-4 and S-5.

Table 2. XRD, FE-SEM, EDAX and AFM details of $Cr_{1-x}W_xN$ films.

Sample name	Chemical Composition (At %)		Grain size (nm)		Lattice constant (A$^{\circ}$)	Surface roughness (nm)
	Cr	**W**	**XRD**	**FE-SEM**		
$Cr_{0.88}W_0N$ (S-1)	88.4	0	31.1	65.2	4.129	14.81
$Cr_{0.61}W_{0.28}N$ (S-2)	61.9	28.6	24.6	51.3	4.144	11.88
$Cr_{0.48}W_{0.43}N$ (S-3)	48.2	43.6	15.2	32.7	4.175	2.11
$Cr_{0.41}W_{0.51}N$ (S-4)	41.3	51.5	17.2	38.9	4.184	7.92
$Cr_{0.28}W_{0.61}N$ (S-5)	28.5	61.2	23.7	50.2	4.187	8.61

It was also observed that the grain size determined by XRD is smaller than the grain size determined by FE-SEM (**Table 2**). This difference in grain size was due to the fact that AFM and FE-SEM show agglomeration of the particles whereas XRD gives an average mean crystallite size. The XRD and FE-SEM/AFM data can be accepted by the fact that smaller primary particles have a large surface energy and would therefore, tend to agglomerate faster and grow into larger grains.

For the quantitative evaluation of surface topography, the average roughness (R_{avg}) of all the thin films was obtained from AFM scans over the substrate area of 1μm×1 μm, three times at a different spot for each thin film by using the relationship,

$$R_{avg} = \frac{1}{N}\sum_{i=1}^{N}|Z_i - \bar{Z}| \qquad (2)$$

where, N is the number of surface height data and $\bar{Z}$ is the mean-height distance. It was found that the surface roughness of $Cr_{1-x}W_xN$ thin films strongly influenced by the W content. The lowest value of surface roughness 2.11 nm was achieved in $Cr_{0.48}W_{0.43}N$ thin film. Further addition of W content after 43.6 % induced higher surface roughness. The kinetic energy of the depositing atom strongly affects the adatoms mobility and formation of the nucleated clusters, which in turn affect the microstructure and surface morphology of the films. As the power rose, the sputtered atoms get more kinetic energy and adatom surface mobility thus nucleation rate is enhanced. High nucleation rate reduces the self-shadowing effect; therefore, the atoms migrate faster on the surface of the substrate. More adatom mobility encourages a more even deposition, so there is a decrease in surface roughness. Higher than 40-watt power, depositing atoms get sufficient energy that they could leave the sites and disturb the evenness of the film so as a result the surface roughness of grown films increased; this change was also explained by others [**19**]. Variation of surface roughness could be described in crystallite size terms, as the crystallite size decreases surface roughness would also decrease due to decrease in the relative grain height therefore small grain size induced low surface roughness. **Table 2** lists all the parameters which were calculated by XRD, FE-SEM and AFM techniques.

Fig. 1 (c) shows the stoichiometric ratio of chromium and tungsten verses power on tungsten target. The composition of the thin films is given in **Table 2** which shows the chromium content decreases and tungsten content increases with the power on the W target. With the increasing power on W target, more W atoms were

sputtered out which replaces the Cr atom and $Cr_{1-x}W_x$ N thin films formed.
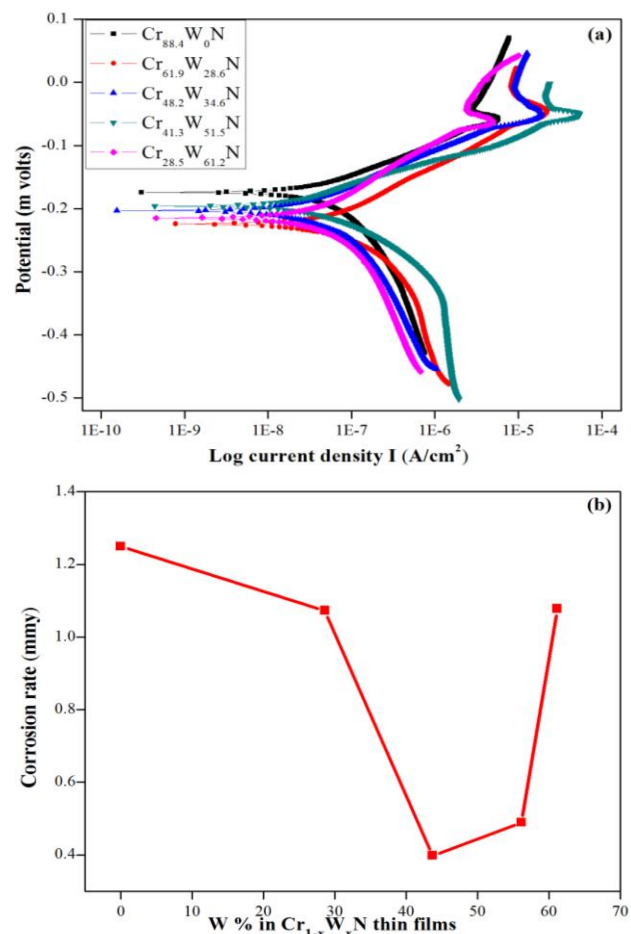
Fig. 3. (a) Potentiodynamic polarization curves and **(b)** Corrosion rate as a function of W % off all the thin films S-1, S-2, S-3, S-4 and S-5 respectively.

Electrochemical properties

Electrochemical techniques widely used for the kinetics study of the electrochemical process in a specific environment. The main motive of our corrosion study is to reduce the corrosion rate by alloying W into CrN matrix. The Tafel Potentiodynamic polarization curves **(Fig.3a)** of all $Cr_{1-x}W_xN$ thin films were estimated from the testing of samples in a3.5% NaCl solution in the open air at room temperature. The corresponding parameters including corrosion current density I_{corr}, corrosion potential E_{corr}, and the most important parameter corrosion rate (CR) are given

in **Table 3**. The performance of the protective coating regarding degradation of the coating material due to the chemical reaction from the relative environment can be described in terms of corrosion rate. The corrosion potential (E_{corr}) and corrosion current density (I_{corr}) were calculated from the intersection of the anodic and cathodic Tafel curves using the Tafel extrapolation method. The shifting of the Tafel polarization curves towards the region of lower current density shows the good corrosion resistance also. Only a factor 3 is estimated between the lowest and highest I_{corr}, it could be due to uncertainly inherent to the Tafel extrapolation method.

Table 3. Potantiodynamic polarization data of the Cr1-xWxN thin films in a 3.5 % NaCl solution.

Sample name	W%	I_{corr} (nA/cm2)	E_{corr} (mV)	Corrosion rate (µmy)
Cr0.88W0N (S-1)	0	240.66	-174	1.248
Cr0.61W0.28N (S-2)	28.61	218.00	-224	1.073
Cr0.48W0.43N (S-3)	43.68	75.66	-194	0.398
Cr0.41W0.51N (S-4)	51.59	92.33	-202	0.497
Cr0.28W0.61N (S-5)	61.21	158.00	-215	1.078

Corrosion rate was determined using CR (mpy) = 0.13 I_{corr} (eq. wt.)/d where eq. wt. and d is the equivalent weight of the material of thin film in grams and density of the films in g/cm^3 respectively. The unit of corrosion rate was converted from mpy (mils penetration per year) to µmy (micrometer penetration per year) using the formula 1 mpy = 25.4 µmy [**20**].

The lowest corrosion rate was found 0.398 µmy in $Cr_{0.48}W_{0.43}N$ thin film compared to other thin films, means this film will degrade only 39.8 nm per year. This corrosion rate value falls in the outstanding region (<25 µm per year) which was suggested by M. G. Fontana [**20**]. Surface roughness plays a very significant role on the corrosion rate of the thin films. In this study, the surface roughness varies with W content and the corrosion rate also follows the surface roughness trend. Modification of corrosion rate of $Cr_{1-x}W_xN$ thin films of lower roughness could be due to the fact that lower roughness provides the higher ratio of real surface area and projected area and lower inhomogeneous surface. Inhomogeneities on the surface might be responsible for weak points that cause corrosive attacks [**21**]. **Fig. 3(b)** depicts the rate of corrosion behavior as a function of W content. The rate of corrosion and surface roughness of the $Cr_{1-x}W_xN$ thin films decreases with the incorporation of W content in the cubic CrN lattice beyond 43.6 %. When this occurs, it is expected that the electrolyte penetrates less easily into the $Cr_{1-x}W_xN$ coatings. Apart from the surface roughness, the enhancement of corrosion rate with the alloying tungsten till 43.6 % may be due to improve covalent bonding character of $Cr_{1-x}W_xN$.

Mechanical properties

Mechanical properties of the $Cr_{1-x}W_xN$ thin films studied by Nanoindentation technique. This technique deals with a nanoindenter tip of known geometry (here we use Verkovich) which is projected onto the selected location on the surface of the material to be tested. As the load increased up to a desired maximum value, the indenter penetrates into the film. After it, removes the load slowly then it was seen that some penetration depth is recovered while some plastic deformation in the sample over there and we get a loading and unloading curve or called p-h curve. As the load is applied, the depth of penetration is measured. The area of contact at full load is determined by the depth of the impression and the known angle or radius of the indenter. The relation between load P and penetration depth h is

$$P = k(h - h_f)^m \qquad (3)$$

where, k and m are power law fitting parameters related to geometric constants, elastic modulus and poison's ratio of the sample and indenter. Hardness is a measure of a material's resistance to surface penetration by an indenter with a force applied to it and defined by the ratio of the maximum load P_{max} to the projected contact area A_c,

$$H = \frac{\epsilon P_{max}}{Ac} \qquad (4)$$

where, ϵ is constant depending upon the geometry of the indenter. The reduced elastic modulus E_r is defined by the given equation,

$$\frac{1}{E_r} = \frac{(1-v_i^2)}{E_i} + \frac{(1-v_s^2)}{E_s} \qquad (5)$$

where, E_i, v_i and E_s, v_s are the elastic modulus and Poisson ratio of the indenter and sample material respectively. The reduced elastic modulus takes into account the fact that elastic displacement occurs in both the thin film specimen and indenter. Reduced elastic modulus attributed by thin film only. The hardness of the thin film coating can be affected by the substrate. Therefore, to avoid this influence the penetration depth should be limited to 1/10 of the film thickness. So that the film deformed by the indenter up to an elastic limit, as a result the indentation data measured the thin film properties with accuracy [**22**].

Hardness (H) and reduced elastic modulus (E_r) have been calculated by directly measuring the physical dimensions of the indentation using the standard method suggested by Oliver and Pharr [**23**] at room temperature. Other important mechanical parameters as plasticity index (H/E) and (H^3/E^2) which is related to the measure of material resistance to the onset of plastic deformation also determined and listed in **Table 4.** The **Fig. 4(a-e)** is showing the loading and unloading curves for $Cr_{1-x}W_xN$ thin films. The hardness and elastic modulus are represented in the **Fig. 4(f)** as a function of tungsten content in $Cr_{1-x}W_xN$ thin films. The measured value of hardness and elastic modulus of $Cr_{0.88}W_0N$ (tungsten content is zero) thin film were 24.80 Gpa and 221.78 Gpa respectively. As W added into CrN up to 28.6 % the hardness and elastic modulus values are increased rapidly up to 33.88 Gpa and 279.06 Gpa respectively i.e. the hardness and elastic modulus increased 73.19 % and 79.47 % correspondingly. In our study, the hardness of $Cr_{1-x}W_xN$ thin films increased as tungsten content reached up to 43.6 %. After that hardness decreases as W content increases in the CrN matrix. It was observed that both the hardness and elastic

modulus follow the same trend as a function of W. Bao-Shun Yau *et al.* [18] has reported that the mechanical properties are widely influenced by the change in charge distribution between W, Cr and N ions accompanying changes in Cr, W and N content. Higher covalent bonding of $Cr_{1-x}W_xN$ thin films exhibits higher hardness then that of more ionic bonding of CrN [8].

Table 4. Mechanical parameters of the $Cr_{1-x}W_xN$ thin films measured by Nanoindentation.

Sample name	Hardness H (Gpa)	Elastic modulus E (Gpa)	H/E 10^{-2}	H^3/E^2 10^{-2} (Gpa)
$Cr_{0.88}W_0N$ (S-1)	24.80	221.78	11.18	31.01
$Cr_{0.61}W_{0.28}N$ (S-2)	33.88	279.06	12.14	49.93
$Cr_{0.48}W_{0.43}N$ (S-3)	43.18	341.02	12.66	69.22
$Cr_{0.41}W_{0.51}N$ (S-4)	37.73	277.24	13.60	69.87
$Cr_{0.28}W_{0.61}N$ (S-5)	35.69	209.80	17.01	103.28

The maximum value of hardness 43.18 Gpa and elastic modulus 341.02 Gpa was achieved in Cr0.48W0.43N thin film, the enhancement in the hardness could be explained by Hall-Petch relation.

$$\sigma_c = \sigma_0 + \frac{k_{gb}}{\sqrt{d}} \quad (6)$$

where, σ_c is critical fracture stress, d is the crystallite size, σ_0 is a material constant for the starting stress for dislocation movement (or the resistance of the lattice to dislocation motion), kgb is the strengthening coefficient (a constant specific to each material). As the load applied on indenter then it penetrates into the material and generate some dislocations inside the crystal, and that influences the properties of the material. Hardness is depending upon the movement of the dislocation from one grain to another grain therefore easy movement of dislocation implies to low hardness.
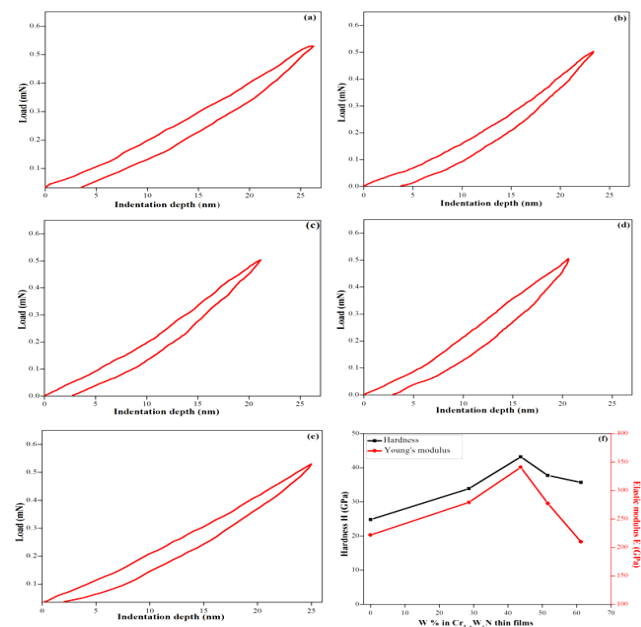
Fig. 4. (a-e) Load versus depth curves and (f) Hardness and elastic modulus as a function of W % of all the thin films S-1, S-2, S-3, S-4 and S-5.

Grain boundaries are behaved like as a barrier that hinders the movement of dislocations from one grain to another grain. Grain boundary fraction volume increases due to the decrease in grain size. The smaller size of grains attributed to restriction in the dislocation movement due to more grain boundary volume thus high hardness achieved by reducing the grain size. Apart from the Hall-Petch relation, residual stress in the thin film also plays a crucial role in deciding the hardness. Higher compressive residual stress is responsible for higher hardness and tensile stress results softness in the thin film. R. whurer *et. al.* [17] has reported that any doped atom larger then host atom it substitutes, generates compressive strain on the surrounding crystal lattice. The atomic radius of W atom (0.169 nm) is larger than the atomic radius of the Cr atom (0.144 nm). Incorporation of W atoms up to 43.6 % in CrN matrix at interstitial position produces compressive stress so the films exhibit higher hardness. Beyond the 43.6 % W content the films exhibit softness comparatively due to dominating of the tensile stress on compressive stress which was generated by the interstitial position of W onto surrounding crystal lattice. The plasticity index (H/E_r) and resistance to plastic deformation (H^3/E_r^2) are also important mechanical parameters for calculating the wear resistance and toughness, respectively. The H/E_r and H^3/E_r^2 values for $Cr_{1-x}W_xN$ thin films are varied in the range (0.1118-0.1701) and (0.3101-1.0328) Gpa respectively, which are indicative of better wear resistance and toughness. Due to high hardness, elastic modulus and good wear resistance these films could be used as protective thin films.

Conclusion

In summary, we have systematically investigated the effect of tungsten content on structural, corrosion and mechanical properties of $Cr_{1-x}W_xN$ (0<x<0.61) thin films. XRD pattern revealed that $Cr_{1-x}W_xN$ films were developed as fcc B-1 NaCl phase with (200) preferred orientation. The XRD peaks shift towards the lower angle with the W content, which attributed to be the expansion of the lattice due to solid solutioning of W in CrN matrix. The crystallite size decreased with increasing W content (power increases to 40 watt) up to 43.6 %, induced high nucleation rate and a reduction of self-shadowing effect of the deposition process. Further increase in W target power results coarse grained structure. Incorporation of W in CrN reduces the surface roughness that exhibits higher ratio of real surface area and projected area and lowers the inhomogeneities on surface, which could be responsible for weak point that offers corrosive attack. The lowest corrosion rate 39.8 nmy was achieved for $Cr_{0.48}W_{0.43}N$ (S-3) thin film. Nanoindentation test revealed that the films exhibit better mechanical properties like hardness and elastic modulus than CrN after W addition in it. It was demonstrated that smooth surface roughness (2.11nm), best corrosion rate (39.06 nmy), highest hardness (43.18 Gpa) and elastic modulus (341.02 Gpa) were achieved in $Cr_{0.48}W_{0.43}N$ thin film. The alloying of W would be great technological interest in order to raise the performance of CrN thin films as protective coatings due to enhancement of structural, surface morphology, electrochemical and mechanical properties.

References

1. Kim, G. S.; Lee, S. Y.; Hahn, J. H.; Lee, B. Y.; Han, J. G.; Lee, S.Y.; Lee, J. H., *Surf. Coat. Technol.* **2003**, *171*, 83.
   DOI: 10.1016/S0257-8972(03)00243-3
2. Zeng, X. T.; Zhang, S.; Sun, C. Q.; Liu, Y.C., *Thin Solid Films.* **2003**, *424*, 99.
   DOI: 10.1016/S0040-6090(02)00921-5
3. Mayrhofer, P. H.; Willmann, H.; Mitterer, C., *Surf. Coat. Technol.* **2001**, *146*, 222.
   DOI: 10.1016/S0257-8972(01)01471-2
4. Hones, P.; Consiglio, R.; Randll, N.; Levi, F., *Surf. Coat. Technol.* **2000**, *125*, 179**.**
   DOI: 10.1016/S0257-8972(99)00541-1
5. Regent, F.; Musil, J.; Surf. Coat. Technol. **2001**, 142, 146.
   DOI: 10.1016/S0257-8972(01)01199-9
6. Sundgren, J. - G.; Hentzell, H. T. G.; J. Vac. Sci, technol. **1986**, A4, 2259.
   DOI: 10.1116/1.574062
7. Bull, S. J.; Jones, A. M.; Surf. Coat. Technol. **1996,** 78, 173.
   DOI: 10.1016/0257-8972(94)02407-3
8. Hones, P.; Zakri, C.; Schmid, P. E.; Levi, F.; Shojaei, O. R.; Appl. Phys. Lett. **2000,** 76, 3194.
   DOI: 10.1063/1.126626
9. Panjan, P.; Navinsek, B.; Cvelbar, A.; Zalar, A.; Milosev, I.; Thin Solid Films.1986, 282, 298.
   DOI: 10.1016/0040-6090(96)08663-4
10. Young, C. E.; Chang, K. M.; Hee, K. D.; Woo, S. D.; Ho, K. K..; J. Mater. Process. Technol, **2007,** 187, 566.
    DOI:10.1016/j.jmatprotec.2006.11.090
11. Wu, F. B.; Tien, S. K.; Duh, J. G., Surf. Coat. Technol. **2005,** 200, 1514.
    DOI: 10.1016/j.surfcoat.2005.08.039
12. Banakh, O.; Schmid, P. E.; Sanjines, R.; Levy, F.; Surf. Coat. Technol. **2003,** 163, 57.
    DOI: 10.1016/S0257-8972(02)00589-3
13. Lee, S. Y.; Kim, S. D,; Kim, G. S.; Hong, Y. S.; Mater. Sci. Forum. **2005,** 486, 444.
    DOI: 10.4028/www.scientific.net/MSF.486-487.444
14. Saha, R.; Inturi, R. B.; Barnard, J. B.; Surf. Coat. Technol. **1996,** 82, 42.
    DOI: 10.1016/0257-8972(95)02624-X
15. Barman, R.; Kaur, D.; J. Alloys Compd. **2015,** 644, 506.
    DOI: 10.1016/j.jallcom.2015.05.047
16. Lousa, A.; Romero, J.; Martinez, E.; Esteve, J.; Montla, F.; Carreras, L.; Surf. Coat. Technol. **2001,** 146, 268.
    DOI: 10.1016/S0257-8972(01)01476-1
17. Kaushal, A.; Choudhary, N.; Kaur, N.; Kaur, D.; Appl. Surf. Sci. **2011,** 257, 8937.
    DOI: 10.1016/j.apsusc.2011.05.068
18. Yau, B. S.; Chu, C. W.; Lin, D.; Lee, W.; Duh, J. G.; Lin, C. H.; Thin Solid Films, **2008,** 516, 1877.
    DOI: 10.1016/j.tsf.2007.10.007
19. Wuhrer, R.; Yeung, W.Y.; Scripta Materialia, **2004,** 50, 813.
    DOI: 10.1016/j.scriptamat.2003.12.022
20. Fontana, M. G.; Corrosion engineering, Macc, Hill, **1987**.
    ISBN: 0-07-021463-8
21. Kumar, A.; Singh, D.; Goyal, R. N.; Kaur, D.; Talenta, **2009,** 78, 964.
    DOI: 10.1016/j.talanta.2009.01.005
22. Veprek, S.; J. Vac. Sci. Technol.; **1999,** A 17, 2401.
    DOI: 10.1116/1.581977
23. Oliver, W. C.; Pharr, G. M.; J. Mater. Res.; **1992,** 7, 1564.
    DOI: 10.1557/JMR.1992.1564

Supporting Information